PHILOSOPHICAL TRANSACTIONS A

rsta.royalsocietypublishing.org

Research

Cite this article: Sclocco R *et al*. 2016 Neuroimaging brainstem circuitry supporting cardiovagal response to pain: a combined heart rate variability/ultrahigh-field (7 T) functional magnetic resonance imaging study. *Phil. Trans. R. Soc. A* **374**: 20150189. http://dx.doi.org/10.1098/rsta.2015.0189

Accepted: 5 January 2016

One contribution of 16 to a theme issue 'Uncovering brain–heart information through advanced signal and image processing'.

Subject Areas:
biomedical engineering, image processing

Keywords:
brainstem, ultrahigh field, autonomic nervous system, pain, functional magnetic resonance imaging, cardiovagal

Author for correspondence:
Roberta Sclocco
e-mail: roberta@nmr.mgh.harvard.edu

†These authors contributed equally to this study.

THE ROYAL SOCIETY PUBLISHING

Neuroimaging brainstem circuitry supporting cardiovagal response to pain: a combined heart rate variability/ultrahigh-field (7 T) functional magnetic resonance imaging study

Roberta Sclocco[1,2,3], Florian Beissner[1,4], Gaelle Desbordes[1], Jonathan R. Polimeni[1], Lawrence L. Wald[1], Norman W. Kettner[3], Jieun Kim[1,5], Ronald G. Garcia[1,6], Ville Renvall[1,7], Anna M. Bianchi[2], Sergio Cerutti[2], Vitaly Napadow[1,3,†] and Riccardo Barbieri[1,2,†]

[1]Athinoula A. Martinos Center for Biomedical Imaging, Department of Radiology, Massachusetts General Hospital, Harvard Medical School, Charlestown, MA, USA
[2]Department of Electronics, Information and Bioengineering, Politecnico di Milano, Milano, Italy
[3]Department of Radiology, Logan University, Chesterfield, MO, USA
[4]Somatosensory and Autonomic Therapy Research, Institute of Neuroradiology, Hannover Medical School, Hannover, Germany
[5]Clinical Research Division, Korea Institute of Oriental Medicine, Daejeon, South Korea
[6]Masira Research Institute, School of Medicine, Universidad de Santander, Bucaramanga, Colombia
[7]Department of Neuroscience and Biomedical Engineering, Aalto University School of Science, Espoo, Finland

RS, 0000-0001-8837-5218

Central autonomic control nuclei in the brainstem have been difficult to evaluate non-invasively in humans. We applied ultrahigh-field (7 T) functional magnetic resonance imaging (fMRI), and the

improved spatial resolution it affords (1.2 mm isotropic), to evaluate putative brainstem nuclei that control and/or sense pain-evoked cardiovagal modulation (high-frequency heart rate variability (HF-HRV) instantaneously estimated through a point-process approach). The time-variant HF-HRV signal was used to guide the general linear model analysis of neuroimaging data. Sustained (6 min) pain stimulation reduced cardiovagal modulation, with the most prominent reduction evident in the first 2 min. Brainstem nuclei associated with pain-evoked HF-HRV reduction were previously implicated in both autonomic regulation and pain processing. Specifically, clusters consistent with the rostral ventromedial medulla, ventral nucleus reticularis (Rt)/nucleus ambiguus (NAmb) and pontine nuclei (Pn) were found when contrasting sustained pain versus rest. Analysis of the initial 2-min period identified Rt/NAmb and Pn, in addition to clusters consistent with the dorsal motor nucleus of the vagus/nucleus of the solitary tract and locus coeruleus. Combining high spatial resolution fMRI and high temporal resolution HF-HRV allowed for a non-invasive characterization of brainstem nuclei, suggesting that nociceptive afference induces pain-processing brainstem nuclei to function in concert with known premotor autonomic nuclei in order to affect the cardiovagal response to pain.

1. Introduction

In recent years, a growing number of studies have investigated the role of different cortical and subcortical brain regions involved in autonomic control during a variety of different tasks and sensory stimuli, and our recent neuroimaging meta-analysis has summarized the diversity of brain regions supporting differential control of the central autonomic network (CAN) [1]. For example, while the amygdala, insula and mid-cingulate cortices were found to form the core of the CAN, regional specificity was found when comparing sympathetic and parasympathetic control networks, as well as when comparing central autonomic response with different tasks and stimuli, such as pain. While the telencephalic and diencephalic circuitry supporting autonomic outflow has been imaged in previous studies, the brainstem circuitry—which includes several important premotor and modulatory autonomic nuclei—has proved more difficult to investigate.

The brainstem acts as a relay and processing station between the spinal cord, cerebellum and neocortex. It contains vital nodes of many functional systems in the central nervous system, including the visual, auditory, gustatory, vestibular, somatic and visceral senses, as well as the autonomic nervous system (ANS). Despite this indisputable importance, the brainstem has been largely neglected in attempts to measure or model brain functions, especially in human neuroscience. One reason for this neglect is that the anatomical characteristics of the brainstem—specifically, its close vicinity to large arteries and ventricles, high levels of physiological noise driven by cardiac pulsatility, the proximity to a steep magnetic susceptibility gradient produced by the air–tissue boundary posterior to the oral cavity and the small size of its nuclei—present inherent challenges to neuroimaging analysis, including functional magnetic resonance imaging (fMRI). Spatial resolution and the signal- or contrast-to-noise ratio, especially using 1.5 T, are typically inadequate for precise brainstem evaluation. Nevertheless, the field of brainstem functional imaging has significantly advanced in recent years, largely due to the development of new investigation and analysis tools that facilitate studying this critical brain structure [2]. Ultrahigh-field fMRI, which allows for improved signal-to-noise ratio and spatial resolution, promises to further our understanding of brainstem and ANS physiology.

Pain is a strong modulator of the ANS, and autonomic dysfunction has been linked with clinically relevant parameters in chronic pain patients, such as fibromyalgia and migraine populations [3–7]. A number of studies have demonstrated that evoked pain stimuli induce increased sympathetic and/or decreased parasympathetic outflows using indirect measures such as heart rate (HR) [8–10], heart rate variability (HRV) [11,12] and skin conductance [13,14]. It is possible that pain-processing nuclei in the brainstem may also be linked with autonomic premotor nuclei, contributing to central autonomic control and to autonomic dysfunction in chronic pain

patients. Exploring the interactions between pain and autonomic modulation in the brainstem is thus highly relevant to clinical applications.

In this study, we use ultrahigh-magnetic-field (7 T) fMRI, a technology with a high signal-to-noise ratio, allowing for improved spatial resolution for an ANS/fMRI analysis focused on the brainstem. Our recent studies have successfully integrated peripheral ANS recordings and fMRI data [15,16] to identify the purported central control regions for autonomic outflow. Our goal here is to investigate specific brainstem nuclei involved in the processing of a strong modulator of autonomic activity, namely evoked pain.

2. Material and methods

Eleven healthy right-handed subjects (8 males, 3 females, 33 ± 4 years old, mean $\pm$ s.d.) were enrolled in the study. All experiments took place at the Athinoula A. Martinos Center for Biomedical Imaging in Charlestown, MA, USA.

(a) Experimental protocol

Subjects experienced fMRI scan runs under a resting or sustained pain condition. For sustained pain, a deep pain sensation was induced by inflating a pressure cuff placed on the subjects' left lower leg (gastrocnemius muscle). Inflation commenced just before each sustained pain run. Prior to the imaging session, the pressure was percept-matched between subjects by asking each subject to signal to the experimenter inflating the cuff when pain was first perceived and then when the pain sensation would be rated as 40 on a scale ranging from 0 (meaning 'no pain') to 100 (meaning 'the most intense pain tolerable'). The calibration procedure was repeated at least three times, and the resulting pressure values were then averaged, in order to ensure a robust estimation. As scans were 6 min in duration, for safety reasons, subjects were instructed to slightly move the toes on their right foot should the pain sensation become too strong during the scan run. This would signal to the investigator to reduce the pressure by 10 mmHg. During the session, participants underwent five fMRI scan runs—three resting-state (hereinafter, REST) runs and two sustained pain stimulation runs (PAIN)—randomized in order and lasting 6 min each. At the end of each PAIN run, subjects were asked to rate the experienced pain intensity on the same 0–100 scale used in the calibration procedure. Ratings were collected retrospectively (i.e. at the end of each PAIN run) regarding both the average pain intensity during the entire run as well as the pain intensities related to three 2-min consecutive windows (initial, middle and final, i.e. each one-third of the entire scan run). Finally, subjects were also asked to rate their average level of anxiety during the PAIN run, on a scale ranging from 0, meaning 'not anxious', to 100, meaning 'very anxious'.

(b) Magnetic resonance imaging and autonomic data collection

Whole-brain blood oxygen level-dependent (BOLD) fMRI data were collected on a Siemens 7 T whole-body scanner (Siemens Healthcare, Erlangen, Germany) using a custom-built 32-channel receive array and birdcage transmit coil [17]. Functional data were acquired with gradient-echo single-shot echo-planar imaging (EPI) using a blipped–controlled aliasing in parallel imaging (blipped-CAIPI) simultaneous multi-slice acquisition [18] with multi-band factor 2 and the following parameters: 1.2×1.2 mm in-plane resolution (field of view $= 192 \times 192$ mm^2), 126 oblique sagittal slices, 1.2 mm slice thickness, repetition time (TR) = 3.5 s, echo time (TE) = 23 ms, flip angle = 80°, no partial Fourier, band width = 1562 Hz pix^{-1}, effective echo-spacing = 0.19 ms, using $R = 4$ in-plane (generalized autocalibrating partially parallel acquisitions (GRAPPA)) acceleration calibrated with 128 fast low-angle excitation echo-planar technique (FLEET) reference lines [19]. In each run, 100 time-series measurements were acquired. For anatomical reference datasets, distortion-matched T1-weighted EPI data (using TR = 8 s, TE = 23 ms, flip angle = 90°, 7/8 partial Fourier) were acquired with a slab-selective adiabatic frequency-offset corrected inversion (FOCI) and a permutation of the temporal ordering of slice acquisition to

achieve 20 inversion times per slice [20]. T1 values were fitted to these inversion recovery curves to produce a T1 map for the image volume, from which a synthetic T1-weighted volume closely resembling the contrast of the Montreal Neurological Institute (MNI) template was generated [21].

Concurrent with BOLD data, peripheral autonomic physiological signals were collected at 400 Hz using a 16-channel Powerlab DAQ System (ADInstruments, Colorado Springs, CO, USA) and the Chart Data Acquisition Software (ADInstruments) running on a conventional Windows OS laptop. In order to estimate the timings of cardiac contraction, a piezo-electric pulse transducer was placed on the index finger of the right hand to record the cardiac pulse signal via blood pressure fluctuation. Respiration was monitored through a custom-built pneumatic belt placed around the subjects' chest/abdomen. Low-compliance tubing connected this belt to an air pressure transducer (PX138-0.3D5 V; Omegadyne, Inc., Sunbury, OH, USA), thereby producing voltage data that corresponded to changes in respiratory volume [22]. Of the original 55 scan runs (11 subjects, five runs per subject), four were discarded due to low-quality pulse pressure signals.

(c) Data preprocessing

(i) Physiological data

Pulse pressure signals were annotated through an automated method followed by manual adjustment, in order to obtain correct peak detection. Beat-to-beat intervals were then fed into a point-process algorithm used to develop local likelihood HR estimation, in order to compute instantaneous estimates of HR and HRV. The previously validated approach models the stochastic structure assumed to generate the pulse pressure peaks as a history-dependent inverse Gaussian process, as its explicit probability density is derived directly from an elementary, physiologically based integrate-and-fire model [23]. The mean of the beat-to-beat interval lengths is modelled as a linear function of the last k beat-to-beat intervals, and this allows for the estimation of the dependence of such intervals on the recent history of parasympathetic and sympathetic inputs to the sinoatrial (SA) node of the heart. Finally, from this set of k regressive coefficients, the total spectral power was computed, and the low-frequency (LF-HRV, 0.04–0.15 Hz) and high-frequency (HF-HRV, 0.15–0.5 Hz) spectral components were extracted. This approach offers the advantage of estimating the dynamics of the model parameters, and, consequently, the time-varying behaviour of the spectral indices, at any time resolution. Thus, the temporal resolution of the HRV index was set to match the temporal resolution of the fMRI signal time series, as detailed below.

As in our previous work [16], the instantaneous HF-HRV index was chosen as a metric for parasympathetic activity, in order to evaluate the modulation induced by sustained pain stimulation on cardiovagal outflow. Furthermore, the adopted point-process approach also provided instantaneous HR estimation. Both HR and HF-HRV series were estimated using a fixed model order $k = 8$, every $\Delta = 2$ ms, low-pass filtered at 0.14 Hz, and resampled at the fMRI TR time points. Each HF-HRV power series went through an additional thresholding below the 98th percentile, in order to remove outlier time-series values, and to normalize the time series to a common peak, thus enhancing sensitivity to the full-range dynamics. The resulting signal was then used as a regressor in the general linear model (GLM) fMRI analysis (see below).

For respiratory data, the maxima and minima for each breathing cycle were identified through an automated method followed by manual adjustment of the respiratory signal, and the changes in the respiration volume per time (RVT) were estimated as in [24], in order to include a regressor of no interest related to respiration activity in the GLM design matrix (see below).

(ii) Magnetic resonance imaging data

The fMRI data were preprocessed using the Oxford Centre for Functional MRI of the Brain (FMRIB) Software Library (FSL; v. 5.0.6) and Analysis of Functional NeuroImages (AFNI) [25]. A first preprocessing stage included image-based retrospective correction (RETROICOR), slice timing correction (using a script developed in-house in order to take into account the simultaneous multi-slice acquisition of our dataset), motion correction and brain extraction. Then,

a spatial preprocessing step was performed, consisting of affine coregistration and nonlinear warping of the T1-weighted EPI to the nonlinear version of the ICBM152 MNI template. The estimated transform matrices were then inverted, in order to be applied to a brainstem mask originally defined in the ICBM152 MNI space, and to transform this mask to the individual functional space. This step was performed in order to mask and retain only the brainstem region from the whole-brain BOLD data, thus reducing the volume of interest in the fMRI analysis and masking out vascular and other non-parenchymal structures surrounding the brainstem, known to be heavily affected by physiological noise [26]. The brainstem mask was taken from Beissner *et al*. [26]. It comprised the entire medulla, pons and mesencephalon and was based on grey and white matter tissue maps of the ICBM152 template thresholded at a tissue probability of 0.9. Finally, minimal spatial smoothing (full width at half maximum (FWHM) = 2 mm) was applied to the BOLD data.

(d) Data analysis

We first evaluated autonomic physiological data to assess whether sustained deep pain altered autonomic activity. Mean HR, HR variance (HRvar), LF-HRV and HF-HRV power, LF/HF ratio and respiration rates were averaged over sessions and across subjects for both REST and PAIN conditions, and statistically tested in order to evaluate the presence of significant differences between the two conditions. As a second step, the indices showing significant changes (i.e. a significant difference between REST and PAIN conditions) were evaluated in the initial, middle and final 2-min windows of the entire 6-min run, in order to estimate temporal variability across the entire 6-min run and identify potential time frames during which a stronger effect was induced. A Kolmogorov–Smirnov test evaluated Gaussianity of the data, and subsequent statistical analyses were performed accordingly. All *post hoc* comparisons were Bonferroni-corrected for multiple comparisons, and the statistical significance threshold was set at $p = 0.05$.

The purported brainstem control nuclei supporting cardiovagal modulation in response to deep pain were obtained using the HF-HRV power series as a regressor of interest in a GLM analysis. The preprocessed parasympathetic measure was convolved with a canonical gamma haemodynamic response function (HRF; SD = 3 s, mean lag = 6 s). In addition to HF-HRV power, two regressors of no interest (cardiac and respiratory activity) were also included in the design matrix, as follows. The HR time series, resampled at the TR of the fMRI acquisition, were convolved with a specific cardiac response function [27] known to reflect the generalized pulsatile artefact resulting from the cardiac contraction pressure wave. Similarly, respiration-related artefacts were reduced by convolving the RVT series with a specific respiration response function [28], and including the result in the design matrix as a second confound regressor. Statistical parametric mapping was carried out using the fMRI Expert Analysis Tool (FEAT v. 6.00; FSL). In the first-level analysis, separate subject-level GLMs were evaluated for each run, for a total of 51 estimations. Parameter estimates derived from each REST and PAIN run were then normalized to MNI space and passed up, with their variances, to second-level fixed-effects analyses for each subject, in order to obtain individual statistical maps for the two examined conditions (leading to 22 second-level estimates). Finally, two group-level mixed-effects analyses (FMRIB's Local Analysis of Mixed Effects (FLAME), FEAT, FSL) [29] produced separate statistical maps for both the REST and PAIN conditions. Furthermore, a REST versus PAIN difference map was evaluated using a paired *t*-test.

Following the results of the 2-min windows analysis of physiological data, BOLD series were similarly split and the same three-level analysis was implemented for specific windows showing a significant effect for HF-HRV modulation. All resultant statistical brainstem maps noted above were corrected for multiple comparisons and family-wise error with a cluster-forming threshold of $Z = 2.3$ and cluster-corrected at $p < 0.05$.

In the 2-min windows analyses, for both autonomic physiological data and ANS/fMRI, we chose to compare PAIN periods with the correspondent REST periods (e.g. initial 2 min of PAIN versus initial 2 min of REST). Thus, in order to rule out potential carry-over effects of pressure

from the preceding PAIN condition on the initial 2-min of REST, both physiological and fMRI data were first tested for the presence of significant variations due to time.

3. Results

(a) Psychophysical and physiological results

All subjects tolerated the sustained pain stimulation procedure. Pressure values used to evoke a deep pain sensation rated as 40 on a scale from 0 to 100 in the PAIN runs ranged between 100 and 240 mmHg (171.82 ± 50.75 mmHg, mean ± s.d.). The pressure estimated through the calibration procedure was used in both PAIN runs or reduced by 10 mmHg in the second run when requested by the subject. Two subjects signalled to reduce the pressure by 10 mmHg during the run. One subject asked for a substantial reduction of pressure (−90 mmHg) for the second PAIN run. This same subject also reported the highest levels of anxiety (60/100 in the first PAIN run, 55/100 in the second run) relative to any other subject and with respect to the average anxiety rating (19.69 ± 22.25), which demonstrated that on average subjects experienced only mild levels of anxiety during scanning.

The average pain ratings (0–100 scale) were significantly higher in the first PAIN run than in the second run (first PAIN run: 49.44 ± 9.45; second PAIN run: 44.62 ± 7.05, paired *t*-test, $p < 0.05$), but no significant differences were found when comparing ratings relative to the consecutive 2-min time windows (first PAIN run: initial 2 min, 45.94 ± 11.72; middle 2 min, 45.62 ± 9.29; final 2 min, 49.69 ± 11.61; second PAIN run: initial 2 min, 43.12 ± 11.93; middle 2 min, 42.5 ± 8.45; final 2 min, 44.37 ± 8.63). Interestingly, a significant reduction in anxiety level was found between the two PAIN runs (first PAIN run: 22.50 ± 22.52; second PAIN run: 16.87 ± 23.13, paired *t*-test, $p < 0.05$), thus suggesting that the reduction in average perceived pain intensity in the second run could be due to a reduction in the anxiety level, or vice versa. Finally, no significant effect for time window was found in the consecutive 2-min ratings, thus allowing us to exclude any temporal summation or adaptation mechanisms in the examined group.

Kolmogorov–Smirnov testing demonstrated lack of Gaussianity for all the autonomic indices considered (HR, HRvar, LF-HRV power, HF-HRV power, LF/HF ratio and respiration rate), thus subsequent statistical analyses were carried out using non-parametric tests. For the initial 6-min run analysis, autonomic indices were compared between REST and PAIN through a Wilcoxon signed-rank test (table 1). A significant decrease during PAIN with respect to REST was found only for HF-HRV power (REST: 1330.89 (336.85;2134.77) ms^2; PAIN: 1012.75 (306.51;1383.3) ms^2; median(interquartile range; IQR), $p = 0.042$) (figure 1*a*). An Ansari–Bradley test also showed a significant reduction in the dispersion of HF-HRV values in PAIN runs with respect to REST ($p \ll 0.001$), demonstrating that a decrease in fluctuation amplitude accompanies the reduction in median values. No significant changes were found for any other indices.

Given the significant effect induced by pain on our index for cardiovagal modulation, we also inspected HF-HRV power for the 2-min time windows, thus dividing the 6-min runs into three consecutive timeframes ('initial', 'middle' and 'final'). A significant effect of time window was confirmed through a Skillings–Mack test [30], used as a substitute for the Friedman test in the presence of an unbalanced design ($p < 0.001$). A first set of *post hoc* comparisons found a lack of significant differences among the three 2-min segments of HF-HRV power during REST, supporting a lack of any potential carry-over effect from preceding PAIN stimulations. Subsequent *post hoc* comparisons showed a significant decrease in HF-HRV power during PAIN with respect to REST in the first 2-min interval (initial-REST: 1486.42(348.66;2409.64) ms^2; initial-PAIN: 890.88(282.6;1581.12) ms^2, $p < 0.05$). No significant differences were found for the second (middle-REST: 1389.44(338.72;2042.82) ms^2; middle-PAIN: 1119.44(291.03;1370.09) ms^2) or the third time window (final-REST: 1125.82(325.03;2128.66) ms^2; final-PAIN: 917.13(365.57;1246.99) ms^2) (figure 1*b*).

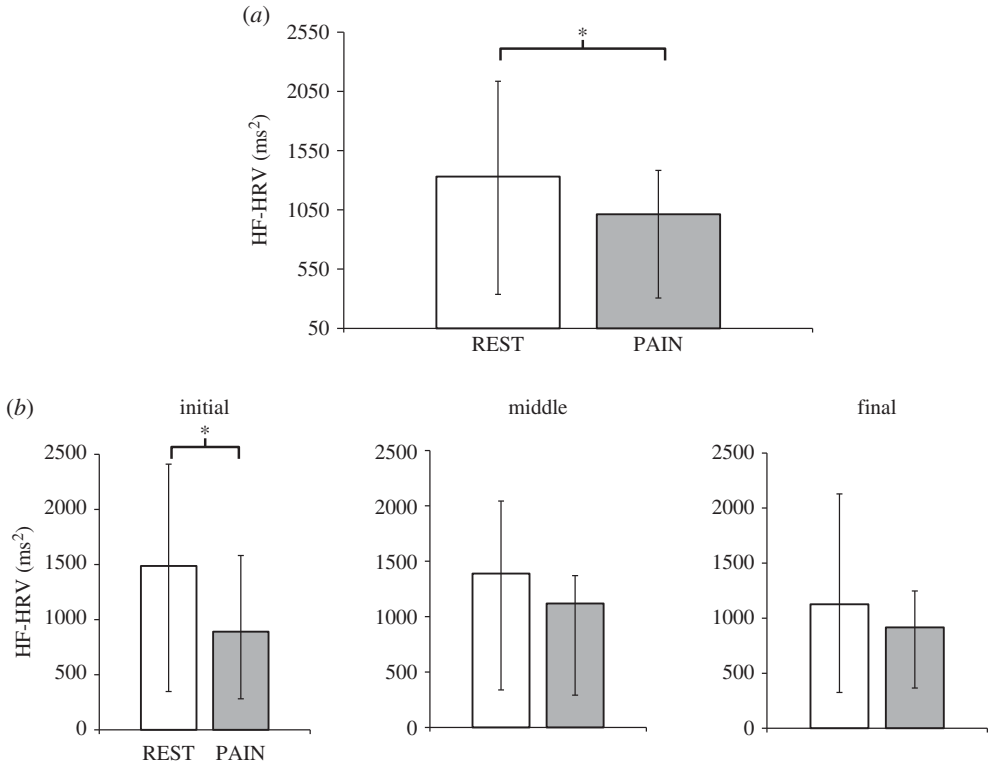

Figure 1. (*a*) Cardiovagal (HF-HRV) response to pain (compared with rest) for the entire 6-min run demonstrated reduced HF-HRV power during PAIN. (*b*) HF-HRV response to pain (compared with rest), evaluated in three consecutive 2-min windows across the entire run, demonstrated reduced HF-HRV power during PAIN for the initial 2-min period only. $^{*}p < 0.05$; statistical significance testing was Bonferroni-corrected for multiple comparisons.

Table 1. Median and interquartile range for autonomic indices during the REST runs and the PAIN runs. Significantly different values (Wilcoxon signed-rank test, $p < 0.05$) between REST and PAIN are reported in italics. bpm, beats per minute; HR, heart rate; HRvar, HR variance; LF-HRV, low-frequency component of heart rate variability; HF-HRV, high-frequency component of heart rate variability.

	REST	PAIN	*p*-value
HR (bpm)	62.85 (60.48;72)	64.22 (60.75;72.6)	0.21
HRvar (bpm^2)	4.04 (2.82;5.49)	3.16 (2.76;3.83)	0.17
LF-HRV (ms^2)	1046.59 (536.98;1405.36)	503.00 (333.93;1367.05)	0.64
HF-HRV (ms^2)	*1330.89 (336.85;2134.77)*	*1012.74 (306.51;1383.3)*	0.04
LF/HF	4.50 (1.23;5.55)	1.61 (0.91;2.75)	0.36
respiration (resp/min)	15.32 (13;18.69)	14.23 (13.63;16.59)	0.96

(b) Autonomic nervous system–functional magnetic resonance imaging analyses

As HF-HRV showed significant pain-evoked modulation (figure 1*a*), this index was used as the regressor of interest in the fMRI data analysis. The differential map resulting from the paired *t*-test between REST and PAIN conditions is reported in figure 2*a*, and the brainstem regions identified are shown in table 2. The significant clusters ($Z > 2.3$, $P < 0.05$) are overlaid on an average of individual functional BOLD images, previously normalized to MNI space. We also report the

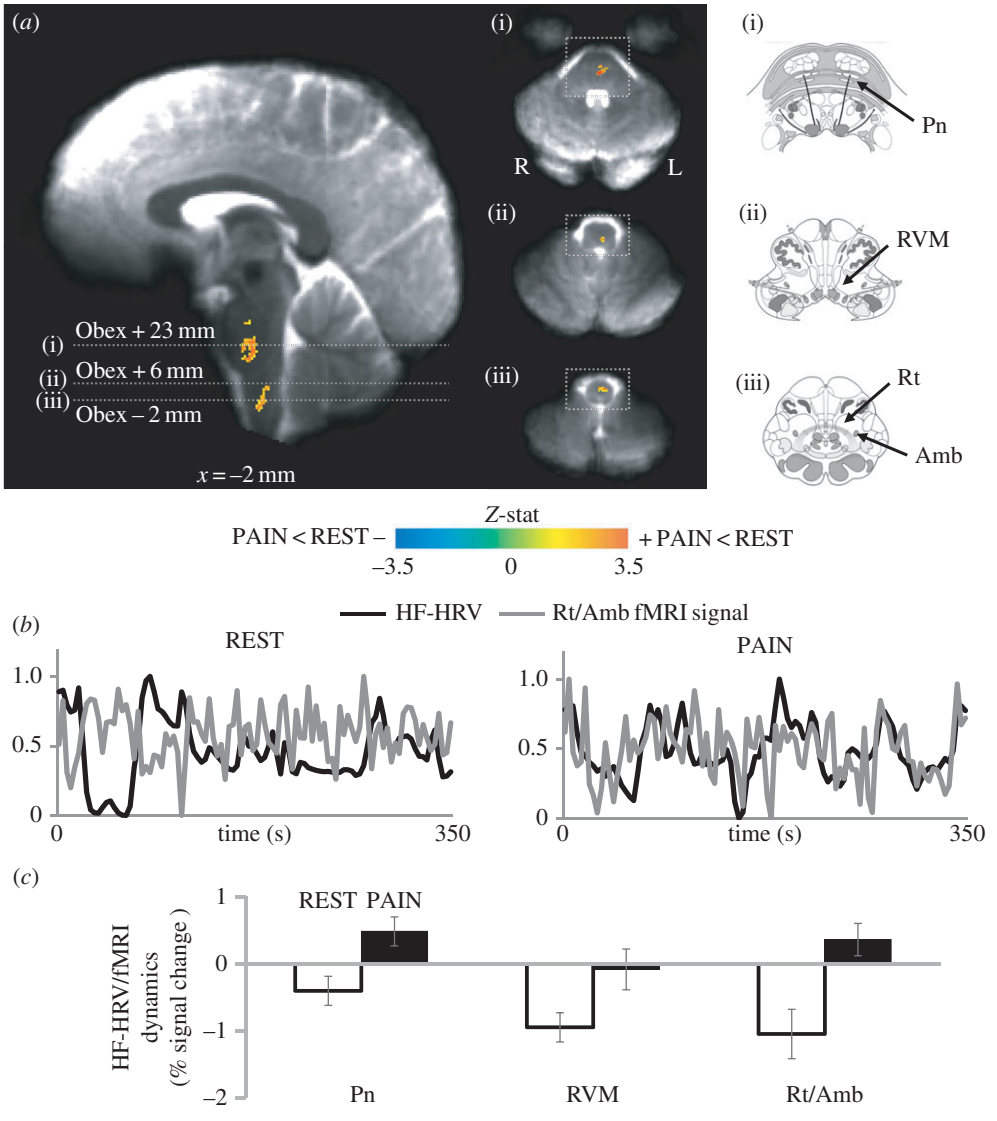

Figure 2. (*a*) Differential map (PAIN–REST) for the HF-HRV/fMRI analysis of the entire (6 min) runs. Group maps are compared with graphical representations of brainstem nuclei as in the Duvernoy atlas [31] (white squares indicate the correspondence on the functional maps). A significant difference between REST and PAIN conditions was found in the pontine nuclei (Pn), the rostral ventromedial medulla (RVM) and the nucleus reticularis medullae oblongatae centralis, including the nucleus ambiguus (Rt/NAmb). (*b*) Normalized values of HF-HRV power (black line) and BOLD signal from Rt/NAmb (grey line) from a representative subject during a REST and a PAIN run. (*c*) Per cent signal change from the significant clusters showing a reduction in the negative correlation (Gi/RVM cluster) or a shift to positive correlation (Pn and Rt/NAmb clusters) during PAIN. Bar plot error bars represent s.e.m.

mean signal intensity response for both REST and PAIN, with an average per cent-change score extracted from a 2 mm radius sphere centred on the peak voxel of each significant cluster. These bar plots show which of the two conditions was driving the significant difference.

For the entire 6-min runs, compared with REST, we found that PAIN produced a reduction in the anti-correlation between HF-HRV and the fMRI signal in a cluster located in the upper medulla, presumably containing the rostral ventromedial medulla (RVM) including the gigantocellular nucleus (Gi) (based on reference atlases [31,32]). At the same time, a switch from anti-correlation to positive correlation was found in a lower medullary region, consistent with the

Table 2. HF-HRV/fMRI analysis: PAIN > REST-associated brainstem regions for the 6-min and the initial 2-min analyses.

		peak location (MNI)			
brainstem region	side	*x*	*y*	*z*	*Z*-score
6-min analysis					
Pn	L	−2	−30	−40	3.96
Pn	L	−6	−20	−31	3.34
RVM	L	−2	−40	−54	3.57
Rt/NAmb	L	−2	−40	−62	3.33
initial 2-min analysis					
LC	R	5	−36	−30	3.59
Pn	L	−5	−21	−29	3.44
Rt/NAmb	L	−1	−41	−53	3.48
Gr/DMNX/NTS	L	−5	−42	−61	3.67

dorsal, intermediate and ventral nucleus reticularis medullae oblongatae centralis (Rt), including the nucleus ambiguus (NAmb), and in two pontine regions consistent with pontine nuclei (Pn) (figure 2*c*). An example of the switch from anti-correlation to positive correlation is shown in figure 2*b*, where the fMRI signal extracted from the Rt/NAmb cluster is plotted together with the HF-HRV power regressor for a representative subject (both time series are scaled between 0 and 1 for visualization).

The same HF-HRV/fMRI differential map was then evaluated in the initial 2-min time window of the runs, when the HF-HRV power showed a significant reduction (figure 2*b*). Also in this case, a residual influence on brain activity during the initial 2 min of REST due to previous painful stimulation was first investigated through an ANOVA for repeated measures including the three consecutive HF-HRV/fMRI maps for each subject. No regions were identified by the analysis; therefore, we evaluated the HF-HRV/fMRI differential map using the initial 2 min of both REST and PAIN. The resulting map (figure 3, table 2) shows a partial overlap with the one obtained by analysing the entire run: significant clusters were found in Pn, in an upper-medullary region including Rt and NAmb, and in the lower medulla, encompassing Rt, NAmb, the dorsal motor nucleus of the vagus (DMNX), nucleus gracilis (Gr) and the nucleus of the solitary tract (NTS). Interestingly, a new cluster, not highlighted by the previous analysis, was also found in the upper portion of the pons, consistent with the locus coeruleus (LC). The anti-correlation between the HF-HRV power and the fMRI signal during REST is confirmed also within the initial 2-min window, as well as the reduction of this anti-correlation or shift to a positive correlative association during PAIN for specific brainstem nuclei (figure 3). No regions were identified by the REST > PAIN contrast, for both the 6-min and the initial 2-min analyses.

4. Discussion

Central autonomic control nuclei in the human brainstem have been difficult to evaluate. Our ultrahigh-field (7 T) fMRI study used a sustained pain stimulus to modulate ANS outflow and applied a combined fMRI/HF-HRV general linear model framework to evaluate putative brainstem nuclei that control and/or sense the cardiovagal modulation induced by deep pain. Physiological data analysis showed a significant reduction of parasympathetic activity (HF-HRV) during PAIN compared with REST runs. Moreover, the pain-induced reduction in HF-HRV was most prominent in the initial 2-min time window during this scan run, and this time frame was further evaluated to determine which brainstem nuclei were associated with reduced cardiovagal

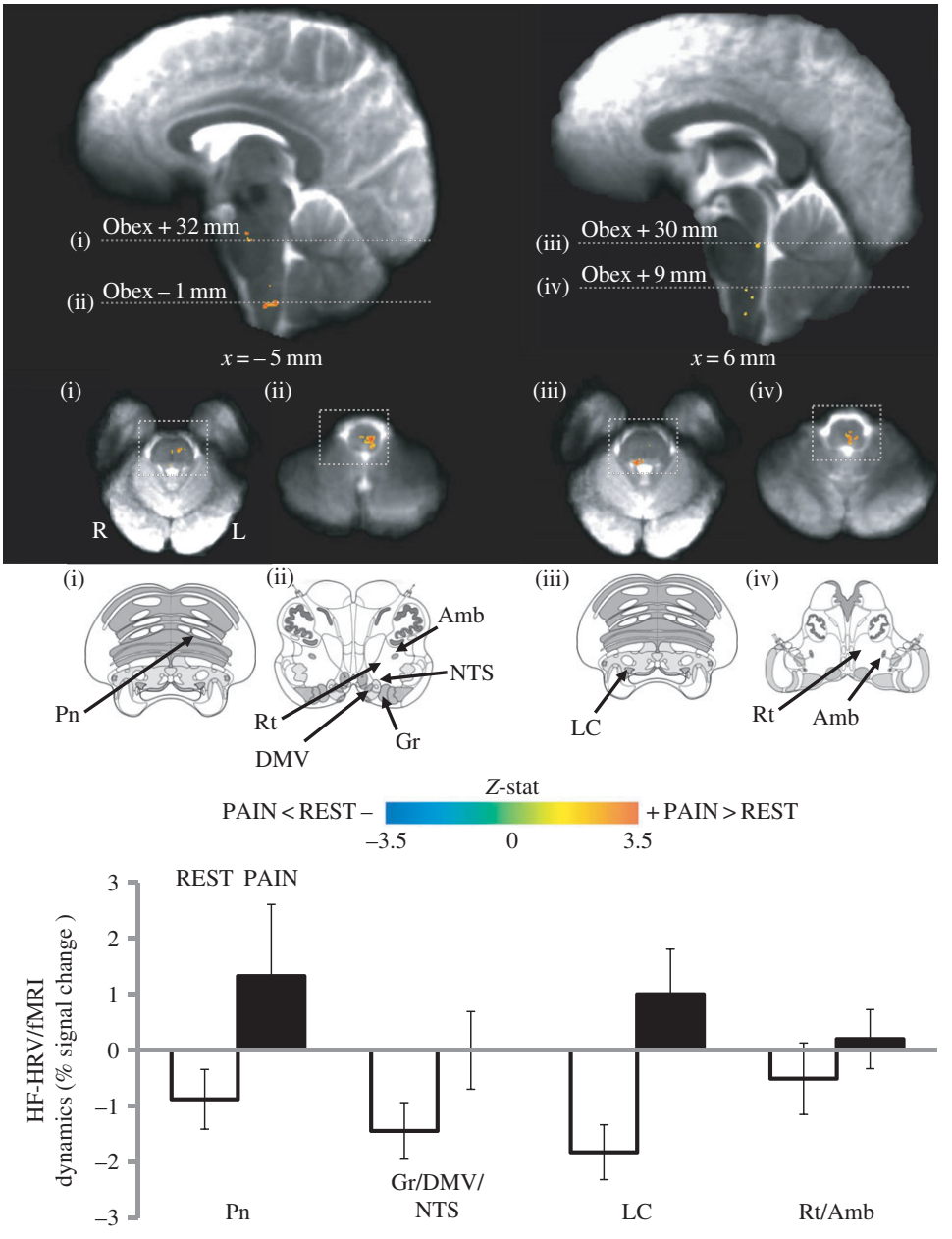

Figure 3. Differential map (PAIN–REST) for the HF-HRV/fMRI analysis of the initial 2-min time window. Group maps are compared with graphical representations of brainstem nuclei from the Duvernoy atlas [31] (white squares indicate the atlas image correspondence on the functional maps). A significant difference between REST and PAIN conditions was found in pontine and medullary regions, including the locus coeruleus (LC) and nucleus of the solitary tract (NTS). Per cent signal change from the significant clusters shows a reduction in the negative correlation or a shift to positive correlation during PAIN. Bar plot error bars represent s.e.m.

outflow. Analysis of the full 6-min scan run found a significant PAIN > REST contrast in several clusters consistent with the RVM, Rt/NAmb and Pn. Analysis of the initial 2-min period of the scan, when HF-HRV was most prominently reduced by PAIN, found a significant PAIN > REST contrast in clusters consistent with the previous 6-min result (Rt/NAmb, Pn), but also identified clusters consistent with DMNX/NTS as well as LC.

The brainstem regions implicated in supporting the cardiovagal response to pain in our study include different structures and nuclei known to be involved in autonomic and nociceptive functions from animal experiments. Both the 6-min and 2-min analyses identified a cluster in the lower pons, which was anatomically consistent with Pn. These nuclei project to the cerebellum and are believed to act as a relay station between the cerebrum and the cerebellum [33]. Furthermore, since Pn also receive projections from hypothalamic and limbic structures, it has been proposed that these connections play a role in the cerebellar contributions to specific cognitive tasks, as well as to the integration of emotional information in movement execution [34]. Recently, an fMRI study reported ventral pons activation ipsilateral to the location of pain in a patient with cluster headache, during typical pain attacks. Given the known projections of these nuclei, the authors hypothesized that Pn are also involved in pain avoidance as they are also associated with the activation of structures involved in motor function and reactive behaviour [35]. A second partially overlapping cluster extended longitudinally in the medulla, and encompassed different nuclei: its upper portion was consistent with RVM including the gigantocellular nucleus (Gi), while its lower portion was localized to the nucleus reticularis (Rt), including the NAmb. For the initial 2-min time window, a similar cluster also included the DMNX, nucleus gracilis (Gr) and NTS, which extends into the dorsolateral medulla. Interestingly, both NTS and Gr are known to receive nociceptive inputs, the former via the vagal nerve and spinal afferents, the latter from the dorsal column pathway [36]. Rt, and particularly its dorsal portion, has also been proposed as a primary pro-nociceptive centre in the brain's endogenous pain modulatory system, integrating multiple excitatory and inhibitory functions for nociceptive processing [37,38]. On the other hand, NAmb and DMNX are both premotor nuclei implicated in the generation of autonomic response patterns evoked by physiological and various sensory stimuli [39]. Both of these nuclei are involved with efferent parasympathetic outflow and play a critical role in parasympathetic reflexes, accepting input from the NTS, which is the principal nucleus for incoming signals, particularly from the viscera via the afferent vagus nerve [40]. Finally, the RVM has been identified as one of the key endogenous pain modulatory areas of the brain, conveying descending pain modulatory influences from the periaqueductal grey to neurons located in the dorsal horn of the spinal cord [41,42]. Thus, it is conceivable that sustained pain stimulation linked pain processing in nociception-associated brainstem nuclei with autonomic response via known autonomic premotor nuclei in the medulla.

Interestingly, the initial 2-min time-window analysis identified another cluster, located in the right upper pons and consistent with the LC. LC is the main source of noradrenaline in the forebrain, and is implicated in autonomic regulation, with an excitatory influence on sympathetic outflow, and an inhibitory influence on parasympathetic outflow [43]. Importantly, the LC also plays a major role in the processing of pain, channelling nociceptive information to the somatosensory cortex and exerting an inhibitory influence on pain sensation [44,45]. Therefore, its involvement in the first minutes of pain stimulation could be interpreted as a coping mechanism in our healthy adult subjects, in an attempt to decrease the pressure-evoked pain sensation.

In both the 6-min and the initial 2-min analyses, we found that an anti-correlation between HF-HRV and the fMRI signal seen during REST was reduced, or even shifted to a positive correlation, during the sustained pain stimulus. In our previous ANS/fMRI study, where we used similar methods to evaluate the CAN response to visual nauseagenic stimulation, this aversive stimulus increased anti-correlation in cortical areas such as the insula [16]. Such common anti-correlations, typically in neocortical regions, may be due to inhibitory links between the identified regions and premotor cardiovagal outflow nuclei (i.e. NAmb). The present brainstem-focused results, which demonstrated that evoked pain induced a positive correlation between the HF-HRV signal and brain activity in important ponto-medullary nuclei such as Pn, LC and most importantly NAmb, suggest that, under sustained nociceptive drive, NAmb activity became in-phase with HF-HRV power, possibly contributing to the decreased cardiovagal modulation induced by this stimulus. However, as NAmb is an elongated nucleus with a very small cross-sectional area in the axial plane ($<1\,mm^2$), future studies may need to push for an even better

spatial resolution and improved temporal resolution to definitely assess the association between NAmb activity and HF-HRV power. Indeed, the modelling of the association between HF-HRV and fMRI signal could be suboptimal, especially in terms of the specific haemodynamic response linking the two signals. Further research should thus explore more precise modelling of the neurovascular coupling/haemodynamic response, leading to a deeper understanding of pain-induced changes in ANS/fMRI analyses.

Interestingly, the two differential (PAIN—REST) analyses, one using the entire run (6 min, figure 2) and the other using the initial 2 min when HF-HRV reduction was most pronounced (figure 3), were partially overlapping, thus suggesting that (i) a 2-min period of data collection contains a high enough signal-to-noise ratio to perform such analyses and (ii) an early, stronger modulation of autonomic outflow may be driving the significant differences found in HF-HRV power and in ANS/fMRI analysis results for the entire 6-min data collection period. This finding also supports the reliability of the time-varying assessment of HF-HRV achievable by the point-process framework, which is able to provide instantaneous estimates (at a temporal resolution matched to the BOLD acquisition time points) within windows as short as 2 min. This may not be true with other approaches, which are based on the assumption of quasi-stationarity across the *entire* time window, typically at least 1 or 2 min in duration. Thus, analysis of the initial 2-min time window, when autonomic outflow was most differentiated between REST and PAIN, supported the specificity of the brainstem nuclei involved as relevant to the control and sensory feedback of cardiovagal modulation by sustained pain stimulation.

Although the results yielded by the two analyses were quite similar, it should be noted that, when the analysis was focused on the specific time window characterized by greater cardiovagal reduction, the differential map demonstrated the involvement of other brainstem nuclei known to be involved in autonomic and nociceptive modulation, not identified when considering the entire length of the run. One possible reason for this result could be neurovascular response habituation to the nociceptive stimulus, leading to attenuation of the BOLD haemodynamic response for this longer time period. Alternatively, specific nuclei such as LC could show a more phasic response, which was only detectable in the initial stage of the stimulation.

While our study successfully identified cardiovagal-associated nuclei in the brainstem response to pain, several limitations should also be noted. The number of subjects was somewhat restricted, and even greater power with a larger cohort may have better identified other brainstem nuclei known from animal models to be related to both pain and cardiovagal outflow/autonomic control, such as the periaqueductal grey. Furthermore, brainstem nuclei typically have a very small cross-sectional area in the axial plane. As different individuals probably have slight differences in the exact location of these nuclei within the brainstem, even if the gross brainstem is perfectly aligned between individuals, and spatial resolution is optimized at ultrahigh-field MRI, spatial smoothing will still be necessary for any group analysis. Future studies may also explore individual subject analyses to further assess CAN physiology, non-invasively, in the human. Second, the anxiety ratings were assessed only at the end of each PAIN run, and not on consecutive 2-min time windows as with the pain intensity ratings. Therefore, it was not possible to control for a potentially increased anxiety level in the first 2 min. On the other hand, on average, subjects experienced only mild levels of anxiety (19.69 ± 22.25, mean $\pm$ s.d., on a scale ranging from 0 to 100), with a significant reduction in the second PAIN run. Thus, the contribution of anxiety level to the examined brainstem activity is likely to be limited. Finally, the pulse signal measured at the finger is about 300 ms delayed with respect to the contraction of the heart. Theoretically, this delay should be incorporated into the HRF convolution used for the HF-HRV GLM regressor to model the BOLD response in the brain. In practice though, this delay should not significantly affect the canonical BOLD HRF, which was used for this study and peaks approximately 5 s after the assumed neuronal activity. A delay (about 150 ms) also exists between vagal nerve activity and cardiac contraction via the sinoatrial node [46,47]. Thus, future modelling should (i) better estimate the HRF in the brainstem and (ii) *explicitly* account for all peripheral delays between neuronal activity and pulse pressure signal recording at the fingertip.

As mentioned in the Introduction, the motivation for conducting this study at 7 T was the increased sensitivity and resolution afforded by ultrahigh-field MRI compared with lower field strengths. Both image signal-to-noise ratio and T2* contrast increase with field strength, therefore the functional contrast-to-noise ratio increases dramatically with field strength [48]. This increased sensitivity to activation can be used to reduce voxel sizes to better sample the small nuclei of the brainstem. However, there are multiple experimental challenges at ultrahigh field strengths. One is increased image distortion in EPI—especially pronounced around air–tissue interfaces such as the oral cavity just anterior to the brainstem. This challenge was mitigated in this study through the use of accelerated parallel imaging [49,50], at the expense of some sensitivity. Another challenge that is particularly relevant to this study is the increased intensity of physiological noise fluctuations with increasing field strength [51]. Physiological noise generated by local magnetic field changes driven by the respiratory cycle are stronger close to the chest [52,53] and therefore are more pronounced in the brainstem than in the cerebral cortex. Fortunately, physiological noise contributions are suppressed in small voxels, where thermal noise dominates [51,54], and previous studies using larger voxels than those employed here demonstrated that approximately 10% of the total noise in the BOLD fMRI time series sampled from the nearby primary visual cortex could be explained by respiratory noise [53]; therefore, this noise source is not expected to contribute much to the total signal variability. A larger concern is the strong cardiac cycle-driven physiological noise, which is prevalent within voxels sampling the brainstem due to partial volume effects between the tissue and surrounding cerebrospinal fluid (CSF), where physiological noise is highest in the brain [55], and this can be a major confound in brainstem fMRI [56]. Smaller voxels also provide reduced partial volume effects that allow tissue signals to be separated from signals emanating from adjacent CSF, as has been demonstrated previously [57]. In this work, the physiological noise sources from within the CSF were explicitly avoided by masking the brainstem, and therefore were largely absent from the fMRI signals. This accurate masking was enabled in part by our use of an anatomical reference dataset with identical distortion to the BOLD fMRI data, namely the T1-weighted EPI. Thus our use of low-distortion, high-resolution fMRI acquisition—enabled by accelerated parallel imaging and the higher sensitivity provided at ultrahigh fields—provided fine sampling of the human brainstem while avoiding noise sources from the surrounding CSF regions.

In summary, successfully exploiting high spatial resolution fMRI and high temporal resolution HF-HRV estimation, this work presents the association between specific areas in the brainstem and pain-induced autonomic modulation. Results demonstrate the existence of a change in the relationship between parasympathetic outflow and numerous brainstem nuclei known to be involved in autonomic regulation and pain processing, mainly located in the medullary and pontine portions of the brainstem.

Ethics. Written informed consent was obtained from all participants, and the protocol was approved by the Human Research Committee of the Massachusetts General Hospital.

Data accessibility. The article's supporting data may be available upon request by emailing the corresponding author.

Authors' contributions. R.S.: acquisition, analysis and interpretation of data, article drafting and final approval; F.B.: conception and design, acquisition of data, manuscript revision and final approval; G.D.: acquisition of data, manuscript revision and final approval; J.R.P.: acquisition of data, manuscript revision and final approval; L.L.W.: conception and design, manuscript revision and final approval; N.W.K.: interpretation of data, manuscript revision and final approval; J.K.: acquisition of data, manuscript revision and final approval; R.G.G.: acquisition of data, manuscript revision and final approval; V.R.: acquisition and analysis of data, manuscript revision and final approval; A.M.B.: interpretation of data, manuscript revision and final approval; S.C.: interpretation of data, manuscript revision and final approval; V.N.: conception and design, acquisition, analysis and interpretation of data, manuscript revision and final approval; R.B.: analysis and interpretation of data, manuscript revision and final approval.

Competing interests. We have no competing interests.

Funding. We thank the following organizations for funding support: Regione Lombardia and Fondazione Cariplo, Project 'THINK&GO' (R.S.); National Institute of Biomedical Imaging and Bioengineering (NIBIB),

NIH: K01-EB011498, Center for Functional Neuroimaging Technologies (J.R.P.), P41-EB015896 (J.R.P., L.L.W.); German Research Foundation grant no. BE4677/1-1 (F.B.); National Center for Complementary and Integrative Health (NCCIH), NIH: K01-AT008225 (G.D.), P01-AT006663 (V.N.), R01-AT007550 (V.N.); National Institute for Arthritis and Musculoskeletal and Skin Diseases (NIAMS), NIH: R01-AR064367 (V.N.); National Institute of Mental Health (NIMH), NIH: R21-MH103468 (R.G.G., V.N.); National Institute of Neurological Disorders and Stroke (NINDS), NIH: R21-MH103468 (V.N.); Instrumentarium Science Foundation, Swedish Cultural Foundation in Finland, Academy of Finland, grant no. 265917 (V.R.). This work also involved the use of instrumentation supported by the NIH Shared Instrumentation Grant Program and/or High-End Instrumentation Grant Program; specifically, grant nos. S10RR019371, S10RR023034, S10RR023401, and S10RR020948.

Acknowledgements. We thank Drs Thomas Witzel and Boris Keil for supporting hardware and software developments for 7 T fMRI.

References

1. Beissner F, Meissner K, Bär K-J, Napadow V. 2013 The autonomic brain: an activation likelihood estimation meta-analysis for central processing of autonomic function. *J. Neurosci.* **33**, 10 503–10 511. (doi:10.1523/JNEUROSCI.1103-13.2013)
2. Beissner F, Baudrexel S. 2014 Investigating the human brainstem with structural and functional MRI. *Front. Hum. Neurosci.* **8**, 116. (doi:10.3389/fnhum.2014.00116)
3. Kim J *et al.* 2015 The somatosensory link in fibromyalgia: functional connectivity of the primary somatosensory cortex is altered by sustained pain and is associated with clinical/autonomic dysfunction. *Arthritis Rheumatol.* **67**, 1395–1405. (doi:10.1002/art.39043)
4. Cohen H, Neumann L, Shore M, Amir M, Cassuto Y, Buskila D. 2000 Autonomic dysfunction in patients with fibromyalgia: application of power spectral analysis of heart rate variability. *Semin. Arthritis Rheum.* **29**, 217–227. (doi:10.1016/S0049-0172(00)80010-4)
5. Reyes del Paso GA, Garrido S, Pulgar Á, Martín-Vázquez M, Duschek S. 2010 Aberrances in autonomic cardiovascular regulation in fibromyalgia syndrome and their relevance for clinical pain reports. *Psychosom. Med.* **72**, 462–470. (doi:10.1097/PSY.0b013e3181da91f1)
6. Al-Din A, Mir R, Davey R, Lily O, Ghaus N. 2005 Trigeminal cephalgias and facial pain syndromes associated with autonomic dysfunction. *Cephalalgia* **25**, 605–611. (doi:10.1111/j.1468-2982.2005.00935.x)
7. Sanya EO, Brown CM, von Wilmowsky C, Neundörfer B, Hilz MJ. 2005 Impairment of parasympathetic baroreflex responses in migraine patients. *Acta Neurol. Scand.* **111**, 102–107. (doi:10.1111/j.1600-0404.2004.00358.x)
8. Hampf G. 1990 Influence of cold pain in the hand on skin impedance, heart rate and skin temperature. *Physiol. Behav.* **47**, 217–218. (doi:10.1016/0031-9384(90)90064-B)
9. Lavigne GJ, Zucconi M, Castronovo V, Manzini C, Veglia F, Smirne S, Ferini-Strambi L. 2001 Heart rate changes during sleep in response to experimental thermal (nociceptive) stimulations in healthy subjects. *Clin. Neurophysiol.* **112**, 532–535. (doi:10.1016/S1388-2457(00)00558-7)
10. Tousignant-Laflamme Y, Rainville P, Marchand S. 2005 Establishing a link between heart rate and pain in healthy subjects: a gender effect. *J. Pain* **6**, 341–347. (doi:10.1016/j.jpain.2005.01.351)
11. Appelhans BM, Luecken LJ. 2008 Heart rate variability and pain: associations of two interrelated homeostatic processes. *Biol. Psychol.* **77**, 174–182. (doi:10.1016/j.biopsycho.2007.10.004)
12. Mostoufi SM, Afari N, Ahumada SM, Reis V, Wetherell JL. 2012 Health and distress predictors of heart rate variability in fibromyalgia and other forms of chronic pain. *J. Psychosom. Res.* **72**, 39–44. (doi:10.1016/j.jpsychores.2011.05.007)
13. Dubé A-A, Duquette M, Roy M, Lepore F, Duncan G, Rainville P. 2009 Brain activity associated with the electrodermal reactivity to acute heat pain. *Neuroimage* **45**, 169–180. (doi:10.1016/j.neuroimage.2008.10.024)
14. Eriksson M, Storm H, Fremming A, Schollin J. 2008 Skin conductance compared to a combined behavioural and physiological pain measure in newborn infants. *Acta Pædiatr.* **97**, 27–30. (doi:10.1111/j.1651-2227.2007.00586.x)

15. Napadow V, Dhond R, Conti G, Makris N, Brown EN, Barbieri R. 2008 Brain correlates of autonomic modulation: combining heart rate variability with fMRI. *Neuroimage* **42**, 169–177. (doi:10.1016/j.neuroimage.2008.04.238)
16. Sclocco R *et al.* 2016 Brain circuitry supporting multi-organ autonomic outflow in response to nausea. *Cereb. Cortex* **26**, 485–497. (doi:10.1093/cercor/bhu172)
17. Keil B, Triantafyllou C, Hamm M, Wald L. 2010 Design optimization of a 32-channel head coil at 7 T. In *18th Annu. Meeting of the International Society for Magnetic Resonance in Medicine* (*Joint Annual Meeting ISMRM-ESMRMB 2010*), *Stockholm, Sweden, 1–7 May 2010*, poster 1493. See http://cds.ismrm.org/protected/10MProceedings/files/1493_6960.pdf.
18. Setsompop K, Gagoski BA, Polimeni JR, Witzel T, Wedeen VJ, Wald LL. 2012 Blipped-controlled aliasing in parallel imaging for simultaneous multislice echo planar imaging with reduced g-factor penalty. *Magn. Reson. Med.* **67**, 1210–1224. (doi:10.1002/mrm.23097)
19. Polimeni JR, Bhat H, Witzel T, Benner T, Feiweier T, Inati SJ, Renvall V, Heberlein K, Wald LL. 2015 Reducing sensitivity losses due to respiration and motion in accelerated echo planar imaging by reordering the autocalibration data acquisition. *Magn. Reson. Med.* **75**, 665–679. (doi:10.1002/mrm.25628)
20. Renvall V, Witzel T, Wald L, Polimeni J. 2014 Fast variable inversion-recovery time EPI for anatomical reference and quantitative T1 mapping. In *22nd Annu. Meeting of the International Society for Magnetic Resonance in Medicine* (*Joint Annual Meeting ISMRM-ESMRMB 2014*), *Milan, Italy, 10–16 May 2014*, poster 4282.
21. Renvall V, Witzel T, Wald L, Polimeni J. 2014 Automatic cortical surface reconstruction and tissue segmentation from high-resolution T1w EPI at 7 T. In *20th Annu. Meeting of the Organization for Human Brain Mapping, Hamburg, Germany, 8–12 June 2014*, poster 3586.
22. Binks AP, Banzett RB, Duvivier C. 2007 An inexpensive, MRI compatible device to measure tidal volume from chest-wall circumference. *Physiol. Meas.* **28**, 149. (doi:10.1088/0967-3334/28/2/004)
23. Barbieri R, Matten EC, Alabi AA, Brown EN. 2005 A point-process model of human heartbeat intervals: new definitions of heart rate and heart rate variability. *Am. J. Physiol.* **288**, H424–H435. (doi:10.1152/ajpheart.00482.2003)
24. Birn RM, Diamond JB, Smith MA, Bandettini PA. 2006 Separating respiratory-variation-related fluctuations from neuronal-activity-related fluctuations in fMRI. *Neuroimage* **31**, 1536–1548. (doi:10.1016/j.neuroimage.2006.02.048)
25. Cox RW. 1996 AFNI: software for analysis and visualization of functional magnetic resonance neuroimages. *Comput. Biomed. Res.* **29**, 162–173. (doi:10.1006/cbmr.1996.0014)
26. Beissner F, Schumann A, Brunn F, Eisenträger D, Bär K-J. 2014 Advances in functional magnetic resonance imaging of the human brainstem. *Neuroimage* **86**, 91–98. (doi:10.1016/j.neuroimage.2013.07.081)
27. Chang C, Cunningham JP, Glover GH. 2009 Influence of heart rate on the BOLD signal: the cardiac response function. *Neuroimage* **44**, 857–869. (doi:10.1016/j.neuroimage.2008.09.029)
28. Birn RM, Smith MA, Jones TB, Bandettini PA. 2008 The respiration response function: the temporal dynamics of fMRI signal fluctuations related to changes in respiration. *Neuroimage* **40**, 644–654. (doi:10.1016/j.neuroimage.2007.11.059)
29. Beckmann CF, Jenkinson M, Smith SM. 2003 General multilevel linear modeling for group analysis in FMRI. *Neuroimage* **20**, 1052–1063. (doi:10.1016/S1053-8119(03)00435-X)
30. Skillings JH, Mack GA. 1981 On the use of a Friedman-type statistic in balanced and unbalanced block designs. *Technometrics* **23**, 171–177. (doi:10.1080/00401706.1981.10486261)
31. Naidich TP, Duvernoy HM, Delman BN, Sorensen AG, Kollias SS, Haacke EM (eds). 2009 Internal architecture of the brain stem with key axial section. In *Duvernoy's atlas of the human brain stem and cerebellum*, pp. 53–93. Vienna, Austria: Springer.
32. Olszewski J, Baxter D. 2014 *Olszewski and Baxter's cytoarchitecture of the human brainstem*, 3rd, revised and extended edition. Munich, Germany: Buttner-Ennever J.A.; Horn A.K.E.
33. Evarts EV, Thach WT. 1969 Motor mechanisms of the CNS: cerebrocerebellar interrelations. *Annu. Rev. Physiol.* **31**, 451–498. (doi:10.1146/annurev.ph.31.030169.002315)
34. Brodal P. 2004 *The central nervous system: structure and function*. New York, NY: Oxford University Press.

35. Morelli N, Rota E, Gori S, Guidetti D, Michieletti E, Simone RD, Salle FD. 2013 Brainstem activation in cluster headache: an adaptive behavioural response? *Cephalalgia* **33**, 416–420. (doi:10.1177/0333102412474505)
36. Willis WD, Al-Chaer ED, Quast MJ, Westlund KN. 1999 A visceral pain pathway in the dorsal column of the spinal cord. *Proc. Natl Acad. Sci. USA* **96**, 7675–7679. (doi:10.1073/pnas.96.14.7675)
37. Paxinos G, Huang X-F, Sengul G, Watson C. 2012 Organization of brainstem nuclei. In *The human nervous system* (eds JK Mai, G Paxinos), pp. 260–327. Amsterdam, The Netherlands: Elsevier.
38. Martins I, Carvalho P, de Vries MG, Teixeira-Pinto A, Wilson SP, Westerink BHC, Tavares I. 2015 GABA acting on GABAB receptors located in a medullary pain facilitatory area enhances nociceptive behaviors evoked by intraplantar formalin injection. *Pain* **156**, 1555–1565. (doi:10.1097/j.pain.0000000000000203)
39. Saper CB. 2002 The central autonomic nervous system: conscious visceral perception and autonomic pattern generation. *Annu. Rev. Neurosci.* **25**, 433–469. (doi:10.1146/annurev.neuro.25.032502.111311)
40. Critchley HD. 2005 Neural mechanisms of autonomic, affective, and cognitive integration. *J. Comp. Neurol.* **493**, 154–166. (doi:10.1002/cne.20749)
41. Silva M, Amorim D, Almeida A, Tavares I, Pinto-Ribeiro F, Morgado C. 2013 Pronociceptive changes in the activity of rostroventromedial medulla (RVM) pain modulatory cells in the streptozotocin-diabetic rat. *Brain Res. Bull.* **96**, 39–44. (doi:10.1016/j.brainresbull.2013.04.008)
42. Gonçalves L, Almeida A, Pertovaara A. 2007 Pronociceptive changes in response properties of rostroventromedial medullary neurons in a rat model of peripheral neuropathy. *Eur. J. Neurosci.* **26**, 2188–2195. (doi:10.1111/j.1460-9568.2007.05832.x)
43. Samuels ER, Szabadi E. 2008 Functional neuroanatomy of the noradrenergic locus coeruleus: its roles in the regulation of arousal and autonomic function part I: principles of functional organisation. *Curr. Neuropharmacol.* **6**, 235–253. (doi:10.2174/157015908785777229)
44. Tsuruoka M, Arai Y-CP, Nomura H, Matsutani K, Willis WD. 2003 Unilateral hindpaw inflammation induces bilateral activation of the locus coeruleus and the nucleus subcoeruleus in the rat. *Brain Res. Bull.* **61**, 117–123. (doi:10.1016/S0361-9230(03)00099-6)
45. Maeda M, Tsuruoka M, Hayashi B, Nagasawa I, Inoue T. 2009 Descending pathways from activated locus coeruleus/subcoeruleus following unilateral hindpaw inflammation in the rat. *Brain Res. Bull.* **78**, 170–174. (doi:10.1016/j.brainresbull.2008.09.005)
46. Spear JF, Kronhaus KD, Moore EN, Kline RP. 1979 The effect of brief vagal stimulation on the isolated rabbit sinus node. *Circ. Res.* **44**, 75–88. (doi:10.1161/01.RES.44.1.75)
47. Levy MN. 1997 Neural control of cardiac function. *Baillières Clin. Neurol.* **6**, 227–244.
48. Wald LL, Polimeni JR. 2015 High-speed, high-resolution acquisitions. In *Brain mapping* (ed. AW Toga), pp. 103–116. Waltham, MA: Academic Press.
49. de Zwart JA, van Gelderen P, Golay X, Ikonomidou VN, Duyn JH. 2006 Accelerated parallel imaging for functional imaging of the human brain. *NMR Biomed.* **19**, 342–351. (doi:10.1002/nbm.1043)
50. Griswold MA, Jakob PM, Chen Q, Goldfarb JW, Manning WJ, Edelman RR, Sodickson DK. 1999 Resolution enhancement in single-shot imaging using simultaneous acquisition of spatial harmonics (SMASH). *Magn. Reson. Med.* **41**, 1236–1245. (doi:10.1002/(SICI)1522-2594(199906)41:6<1236::AID-MRM21>3.0.CO;2-T)
51. Triantafyllou C, Hoge RD, Krueger G, Wiggins CJ, Potthast A, Wiggins GC, Wald LL. 2005 Comparison of physiological noise at 1.5 T, 3 T and 7 T and optimization of fMRI acquisition parameters. *Neuroimage* **26**, 243–250. (doi:10.1016/j.neuroimage.2005.01.007)
52. Bianciardi M, Evans KC, Polimeni JR, Song TY, Keil B, Witzel T, Rosen BR, Boas DA, Wald LL. 2013 Investigation of cardiac and respiratory pressure waves in the brain by high resolution echo-planar imaging at 7 Tesla. In *ISMRM 21st Annu. Meeting & Exhibition, Salt Lake City, UT, 20–26 April 2013*, poster 3254.
53. Bianciardi M, Fukunaga M, van Gelderen P, Horovitz SG, de Zwart JA, Shmueli K, Duyn JH. 2009 Sources of functional magnetic resonance imaging signal fluctuations in the human brain at rest: a 7T study. *Magn. Reson. Imaging* **27**, 1019–1029. (doi:10.1016/j.mri.2009.02.004)

54. Triantafyllou C, Polimeni JR, Wald LL. 2011 Physiological noise and signal-to-noise ratio in fMRI with multi-channel array coils. *Neuroimage* **55**, 597–606. (doi:10.1016/j.neuroimage.2010.11.084)
55. Bodurka J, Ye F, Petridou N, Murphy K, Bandettini PA. 2007 Mapping the MRI voxel volume in which thermal noise matches physiological noise—implications for fMRI. *Neuroimage* **34**, 542–549. (doi:10.1016/j.neuroimage.2006.09.039)
56. Brooks JC, Faull OK, Pattinson KT, Jenkinson M. 2013 Physiological noise in brainstem fMRI. *Front. Hum. Neurosci.* **7**, 623. (doi:10.3389/fnhum.2013.00623)
57. Satpute AB, Wager TD, Cohen-Adad J, Bianciardi M, Choi J-K, Buhle JT, Wald LL, Barrett LF. 2013 Identification of discrete functional subregions of the human periaqueductal gray. *Proc. Natl Acad. Sci. USA* **110**, 17 101–17 106. (doi:10.1073/pnas.1306095110)